Master's Thesis of Engineering

Fabrication of Organic Transistors Based on N-Type Polymer Semiconductors and Their Applications in Stretchable Photodetectors

N형 고분자 반도체 기반 유기 트랜지스터 제조 및 신축성 광센서에서의 응용

August 2021

Graduate School of Chemical and Biological Engineering
Seoul National University
Polymers and Organic Materials Major

Jong Min Park

Fabrication of Organic Transistors Based on N-Type Polymer Semiconductors and Their Applications in Stretchable Photodetectors

Advisor Joon Hak Oh

Submitting a master's thesis of
Engineering

August 2021

Graduate School of Chemical and Biological Engineering
Seoul National University
Polymers and Organic Materials Major

Jong Min Park

Confirming the master's thesis written by
Jong Min Park
August 2021

Chair	Dongwon Yoo
Vice Chair	Joon Hak Oh
Examiner	So Youn Kim

Abstract

Regio-regularity can affect electrical, mechanical, and optoelectrical properties by changing the microstructure of polymer semiconductors. In this study, PCDT-TIC (PC) and PIDT-TIC (PI), as novel n-type polymer semiconductors, were synthesized, and the impact of regio-regularity on various properties was analyzed. In the case of electrical properties, regio-regular (RR) polymers exhibited superior electrical mobility than regio-random (RA) polymers because charge transfer is advantageous due to their relatively high crystallinity (5.9×10^{-2}, 8.6×10^{-2} $cm^2 V^{-1} s^{-1}$ for PC-RR and PC-RA, respectively, and 1.2×10^{-2}, 1.0×10^{-2} $cm^2 V^{-1} s^{-1}$ for PI-RR and PI-RA, respectively). In the case of mechanical properties, the elastic moduli of RA polymers were significantly lower than those of RR polymers, and diamond-shaped microvoids were generated at stetching of 100% for PC-RR, whereas it was observed at stetching of 150% for PC-RA. Furthermore, as a result of evaluating electrical properties by fabricating an organic field-effect transistor with a 100% stretched polymer film, PC-RR and PC-RA showed 90% and 33% electron mobility retention, respectively. Also, in the case of optoelectrical properties, PC-RR showed higher R, EQE, and D* than PC-RA. Also, PC-RR showed higher R, EQE, and D* than PC-RA. In particular, the PC-RR polymer-based phototransistors were able to maintain optoelectronic properties even at stretched conditions even at NIR wavelengths.

Keyword : Organic Field-Effect Transistors, Stretchable Device, Organic Phototransistors, Regio-regularity, NIR Photodetector, N-type Polymer Semiconductor.

Student Number : 2019-21299

Table of Contents

List of Figures and Tables

Chapter 1. Introduction

Chapter 2. Electrical Characteristics of Stretchable Organic Field-Effect Transistors under Mechanical Strain

Chapter 1. Introduction

1.1. Organic Field-Effect Transistors

Organic field-effect transistor (OFET) has attracted technological interest due to its competitive advantages including easy fabrication, low-cost, light-weight, easy to control electrical, optoelectrical, and mechanical properties through the molecular design, and application potential as a flexible device.[1-4] The organic semiconductors, which have a variety of fabrication methods (vacuum deposition, solution process[5-7], and single-crystal growth[8]), have great potentials such as memory devices[9-11], sensors[12-15], and wearable devices.[16, 17] OFETs consist of semiconducting layer, a dielectric layer, source/drain electrodes, and a gate electrode. Based on these components, the geometric structure of OFETs can be classified into 4 categories (**Figure 1.1**). In these geometric structures, the gate electrode is isolated from the semiconducting layer by the dielectric layer to control the source-drain current (I_{DS}). When the voltage is applied between source and gate electrodes (V_{GS}) and reached a threshold voltage (V_T), the charges are localized at the dielectric layer and form the conducting channel of charge carriers in a semiconducting layer. The charge transport channel between source and drain gates can be controlled by applying V_{GS}. (**Figure 1.2**). When ($V_{GS} - V_T$) > V_{DS} situation, the I_{DS} increase linearly V_{DS} and this region is called a *linear region*. When the V_{DS} exceeds $V_{GS} - V_T$, the channel is *pinch-off*. Therefore, the charge carrier depletion region is observed near the drain electrode. After that, if the V_{DS} further increased, the depletion region extended slightly. Therefore, the I_{DS} is saturated, and this region is called the *saturation region*. Equation (1) and (2) define I_{DS} in the linear and saturation regimes, respectively.

$$I_D = \frac{W}{L} C_i \mu \left(V_{GS} - V_T - \frac{V_D}{2} \right) V_{Ds}, |V_{DS}| < |V_{GS} - V_T| \quad (1)$$

$$I_D = \frac{W}{2L} C_i \mu (V_{GS} - V_T)^2, |V_{DS}| > |V_{GS} - V_T| \quad (2)$$

Where, W is the channel width, L is the channel length, C_i is the capacitance of the dielectric and μ is the field-effect mobility.

1.2. Stretchable Electronic Materials

Stretchable device means electronic devices or materials which can maintain their properties under highly stretched condition. There are two kinds of materials have been studied to make a stretchable device. One is inorganic and the other is organic. Inorganic materials such as silicon and metals are rigid and brittle in bulk form. Organic materials are soft and ductile. To solve the inorganic material's original properties, various strategies have been studied. The representative approach is an island-type of a composite of inorganic nanoparticles in organic elastomers.[18] On the contrary, organic materials can be changed their properties by molecular design. Also, they can be fabricated the simple ways such as solution process and ink-jet printing.[19] However, the mechanical properties of organic materials are still a critical issue.[20-22]

For fabricating highly stretchable OFET, there are three representative strategies considered. Geometric structural design is usually used to improve the stretchability of electrodes.[23] The stretchable electrode should exhibit almost no change in electrical properties at stretched states. Buckled or waved pattern[24-26], micro-cracked[27], or porous[28-30] structures have been applied. Another strategy is to design of stretchable devices. The first is to develop stretchable conductors as a linker between the rigid devices and substrate.[31] Second is to molecular design for high stretchability intrinsically. This strategy can be applied to all components of OFET such as substrate, dielectric, electrode, active layer.[22, 23, 32-37]

Basically, rigid and brittle materials can't be used for highly stretchable electronic devices. However, by changing their geometric structure, all materials can improve their intrinsic stretchability. Therefore, stiff materials can be used as components of stretchable

devices. **Figure 1.3** shows the scheme of the geometric structure change effect. When strain is applied, the energy can be well dissipated by changing the geometric structure. Therefore, 1D stiff materials patterned wavy structure can be more stretched without crack. The effect of the mesh network is shown.[38] Inorganic materials can be stretched in a wavy patterned network. In a patterned network, the wavy line can more improve the stretchability than a straight-line network. This strategy is usually used when using an inorganic electrodes or low stretchable material.

The island-type devices were fabricated for using inorganic material in stretchable displays. However, at the edge of the island, the strain was localized. Therefore, the rigid island device is damaged eventually.[39] To solve this problem, active materials are deposited onto a pre-strained substrates. Pre-strain is released, the substrate is wrinkled in the out of the plane. The buckled structures can resist strain by dissipating the strain while changing their shapes. Although these geometric engineering strategies may afford improved stretchable electronic devices, it should be considered device density and additional process.[40]

As the last strategy to improve the stretchability, intrinsically stretchable material design with high device density and easy fabrication process has been actively studied.[41] By using this strategy, intrinsically stretchable semiconductors can be directly patterned and transferred on the substrate to increase device density (**Figure 1.4**). To improve the intrinsic stretchability, various energy dissipating elements such as dynamic bond[41-44], nanoconfinement[41], nearly amorphous microstructure[16, 45], soft cross-linker[46], and side-chain engineering [47, 48]are required. In particular, the intrinsically stretchable semiconductor development is a charming strategy because polymers can control their electronic properties by molecular design and have relatively low tensile modulus. In addition, polymer semiconductors have shown similar skin characteristics such as self-healing and biocompatible devices.[49-51]

1.3. Organic Phototransistors

The photodetector absorbs the energy of the irradiated photons and transforms it as current. The photo-induced current increased as the charge is excited with no recombination (**Figure 1.5**).[52] To estimate the optoelectronic properties, there are 4 representative parameters such as photoresponsivity (R), photocurrent/dark current ratio (P), external quantum efficiency (EQE, η), and detectivity (D^*). The R and P values are calculated via eq 2 and 3[53]

$$R = \frac{I_{ph}}{P_{in}} = \frac{I_{light} - I_{dark}}{P_{in}} \quad (2)$$

$$P = \frac{I_{light} - I_{dark}}{I_{dark}} \quad (3)$$

Where I_{ph} is the photocurrent, P_{in} is the incident light intensity, I_{light} is the drain current when the light is irradiated to the OPTs, and I_{dark} is the current measured in the dark condition. Also, the EQE and D^* values can be calculated via eq 4 and 5

$$\eta = \frac{(I_{light} - I_{dark})hc}{eP_{int}A\lambda_{peak}} = \frac{R\hbar\nu}{q} \quad (4)$$

$$D^* = \frac{\sqrt{A}}{NEP} = \frac{R}{\sqrt{2eI_{dark}/A}} \quad (5)$$

Where h is the Plank constant, c is the speed of light, e is the fundamental unit of charge, A is the channel domain of the device, λ_{peak} is the specific wavelength of light, and q is the elementary charge. In eq 5, where A is the active device area of the photodetector, NEP is known as noise equivalent power.

By using organic photo-transistors (OPTs), the gain values can be increased due to their additional gate which induces the internal photoconductive gain.[54, 55]Without applying V_{GS}, the phototransistors show the same behavior as a photodiode. [56-59]

1.4. Research Objectives

An amorphous polymer-based organic field-effect transistor was fabricated through molecular design, and electrical properties were analyzed according to stereoregularity. As a result, regio-regular polymer showed better electrical properties than regio-random polymer due to their charge transporting ability. Also, through the soft contact lamination method, it was confirmed how the difference in crystallinity due to stereoregularity affects the retention of the electrical characteristics in the 100% stretched state. After that, polymer crack onset strains were analyzed by polarized UV and optical image monitoring. The regio-random polymer films showed high stretchability with 90% mobility retention under 100% strain due to its amorphous region acting as an energy dissipation region. The characteristics of the phototransistor in the NIR region wavelength band were evaluated by examining the maximum absorption wavelength band that was later confirmed through UV/visible spectroscopy analysis. Furthermore, it was shown through photo-switching that the optical characteristics can be maintained even with mechanical deformation. In this research, we develop and evaluate materials with potential that can be applied as next-generation wearable devices and health monitoring sensors, based on substances that exhibit optical properties while being intrinsically stretchable.

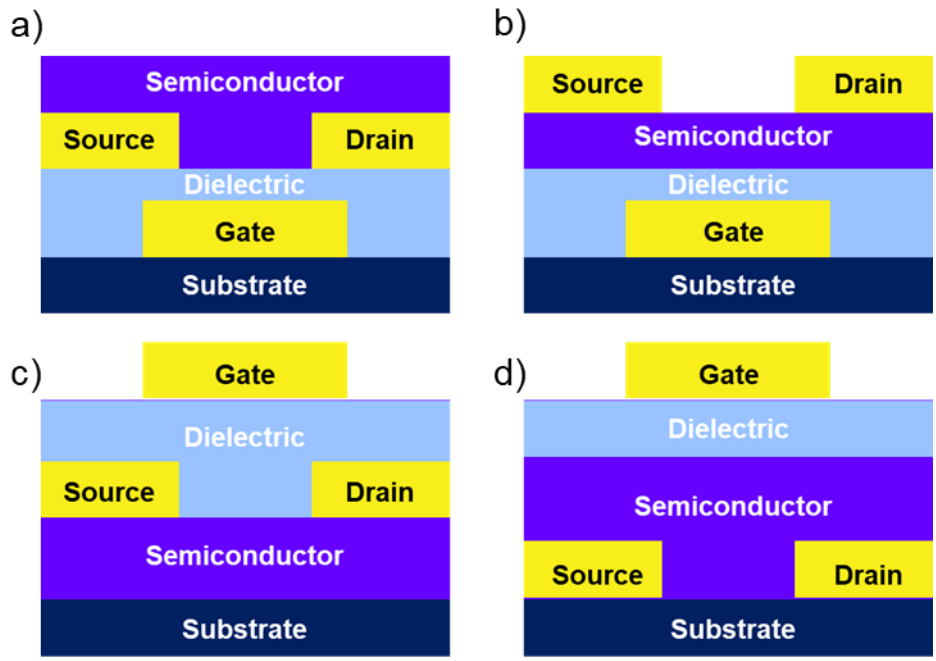

Figure 1.1. Four representative geometric structure of field effect transistors: a) bottom-gate/bottom-contact (BGBC), b) bottom-gate/top-contact (BGTC), c) top-gate/top-contact (TGTC), d) top-gate/bottom-contact (TGBC).

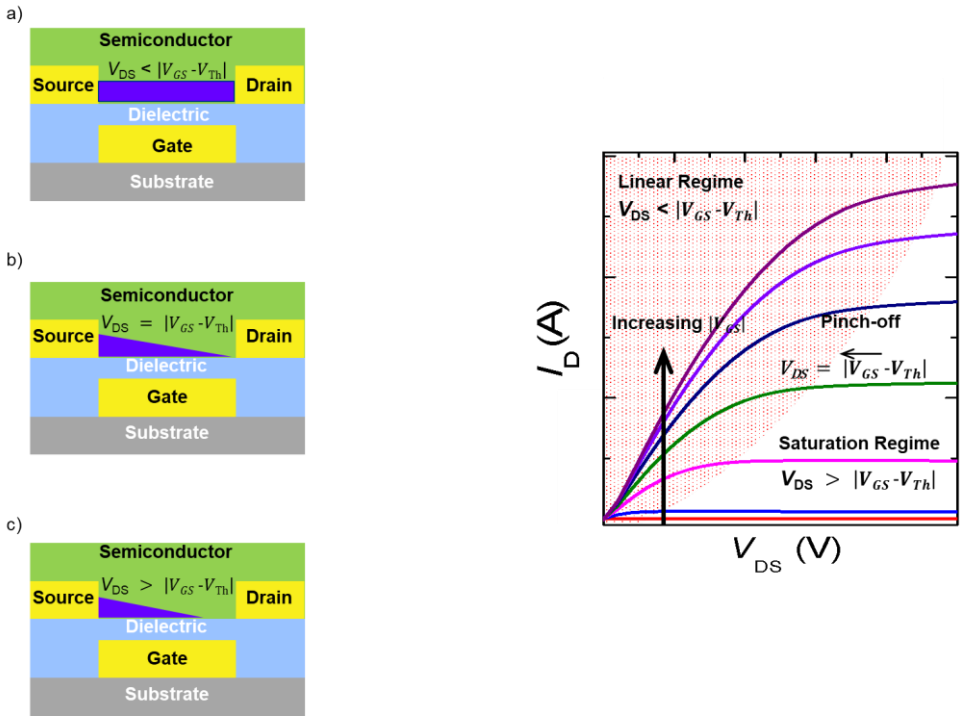

Figure 1.2. Schematic of the OFET operation with *p*-type semiconductor (left) and ideal output characteristics of OFETs (right). a) schematic of carrier concentration in the linear regime, b) schematic of carrier concentration when the pinch-off occurs, c) schematic of carrier concentration in the saturation regime.

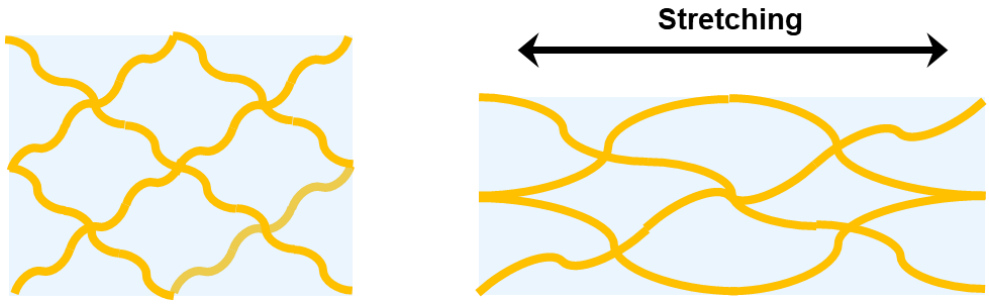

Figure 1.3. Schematic of geometric structure control for stretchable device.

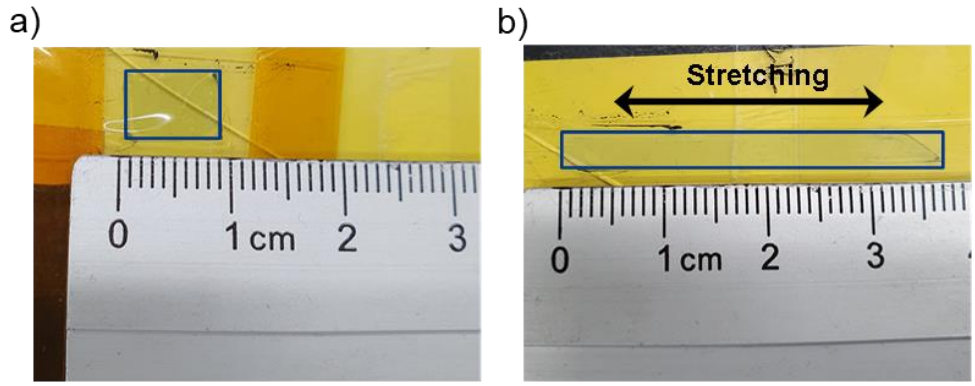

Figure 1.4. Optical images of intrinsically stretchable polymer semiconductor polymer film a) 0% stretched state film, b) stretched state film.

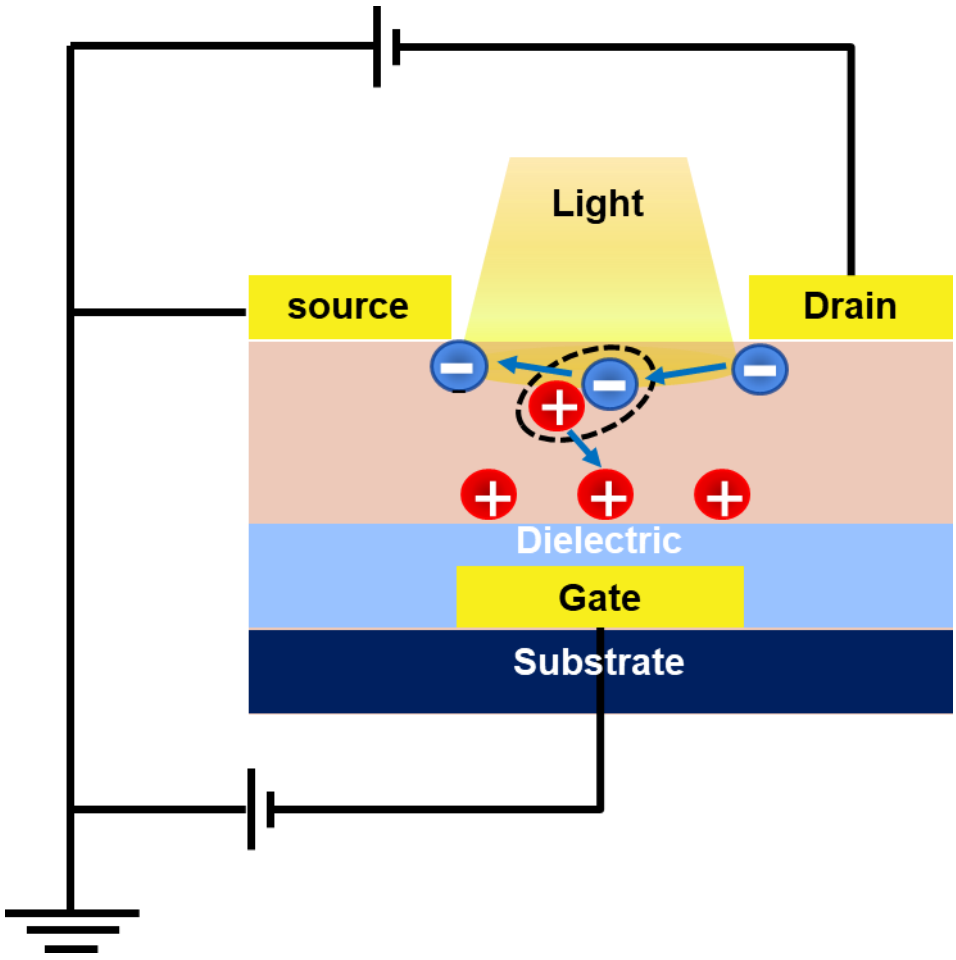

Figure 1.5. Schematic of operation mechanism of organic photo-transistors.

Chapter 2. Electrical Characteristics of Stretchable Organic Field-Effect Transistors under Mechanical Strain

2.1. Introduction

Polymer semiconductors are usually used as active layers in electronic skin due to their softness. However, stretchable polymer semiconductors have a trade-off relationship between electrical characteristics and stretchability. The amorphous domains can dissipate the stress, and crystalline domains can improve the charge mobility. O'Connor et al. researched the mechanical and electrical properties by comparing P3HT with PBTTT. PBTTT has more crystalline domains than P3HT. As a result, the P3HT has higher crack onset strain, lower modulus, but lower mobility.[39] And also, highly regio-regular P3HT has shown large anisotropic charge-transport characteristics because the polymer chain is aligned to the direction of strain. For this reason, parallel direction mobility is much higher than perpendicular direction. To improve the stretchability, there are still lots of approaches such as side-chain engineering,[60] soft cross-linker inducing,[61] dynamic bonding,[62] and nanoconfinement[41]. These strategies can improve the stretchability of the device without compromising mobility. For example, research of side-chain engineering effects on the mechanical properties showed that bulk side chains induced lower elastic modulus, and crack is generated under the strained state because of their increased amorphous region. DPP polymer added PDMS cross-link agent is exhibited crack onset strain exceeding 100% strain. Although being cross-linked, the films have a lower modulus than the original one because of the softness of cross-linking agent. DPP-based polymers induced hydrogen bonding units were reported as high stretchable materials. However, this improved stretchability is compromised with charge mobility. Moreover, 10 mol% of hydrogen bonding units were shown to improve stretchability without any decreasing charge

mobility.

The chain properties can be modified using nanoconfinement. Polymer chains changed more dynamically under nanoconfinement conditions, Nanoconfined semiconductors were exhibited crack onset strains above 100% and maintained their mobility under 100% strain.[63] Moreover, the mobilities of the nanoconfined polymer semiconductor can be improved up to 5 $cm^2\ V^{-1}\ s^{-1}$ by using the solution shearing process.

2.2. Experimental Section

2.2.1. Fabrication of OFETs and electrical characteristics

Commercially available, highly n-doped (100) Si wafers, with thermally grown SiO2 (300 nm; C_i = 11.5 nF cm^{-2}), were used as substrates and gate dielectrics for bottom-gate top-contact (BGTC) structure OFETs. The SiO_2 surfaces were modified with a self-assembled monolayer (SAM) composed of OTS according to a previously reported procedure. The polymers were dissolved in chloroform (2 mg mL^{-1}), and the solutions were stirred for 6 h. After that, the polymer solutions were spin-coated at 2000 rpm for 1 min on the OTS treated SiO_2/Si wafers. Then, the wafers were annealed at 100°C for 10 min. For BGTC OFETs, 40 nm gold source and drain electrodes were thermally evaporated on the polymer films. By using a shadow mask, the channel length (L) and width (W) are 50 μm and 1000 μm, respectively.

The field-effect mobility in the saturation region was calculated by the following equation:

$$I_D = \frac{W}{2L} C_i \mu (V_{GS} - V_T)^2, |V_{DS}| > |V_{GS} - V_T|$$

Where, W is the channel width, L is the channel length, C_i is the capacitance of the dielectric and μ is the field-effect mobility. All electrical properties of the OFETs was measured by using Keithley 4200 semiconductor parametric analyzer in an N_2 atmosphere.

2.2.2. Electrical Characteristics of OFETs under Stretched

Conditions

To characterize the electrical performance of the OFET according to the stretched conditions, the polymer solution (2mg/ml, in chloroform) was stirred overnight at 50℃. After that, the polymer films were formed by spin-coating process onto OTS treated SiO2/Si wafer. These polymer films were transferred onto the PDMS (20:1, base to cross-linker mass ratio), and the films were stretched onto PDMS. Then, these stretched films were directly laminated onto the SiO2/Si wafer by soft contact lamination method[64]. After that, 40 nm gold source and drain electrodes were thermally evaporated on the stretched films. The electrical characteristics of the stretched film based OFETs were measured using a Keithley 4200 semiconductor parametric analyzer.

2.2.3. Mechanical Characterizations

The elastic modulus of polymer films was calculated by using nanoindenter (NX-10, Park Systems) and the Berkovich tip was used to compress the sample. The Oliver-Pharr method was used to define the elastic modulus and the Poisson's ratio value is set as 0.5 for all calculations. The thin films of polymer were spin-coated onto OTS treated SiO_2/Si wafer. Each polymer was indented 10 points and the average value of elastic modulus was reported.

To measure the crack onset strain, the dichroic ratio by using polarized UV/vis spectroscopy (JASCO, V-770) was calculated. In the absorption analysis, Quartz crystal was measured as baseline, and PDMS (Sylgard 184, Dow Corning, cured at 70℃) was measured twice according to stretching direction. The spin-coated polymer films were transferred onto PDMS and stretched. The polarized UV/visible spectroscopy was investigated twice under the mechanical strain.

Optical microscopy (OLYMPUS, BX53) monitoring was performed to prove the crack onset strain. The transferred polymer

films onto the PDMS substrate were stretched from 0 to 100% strain using a custom-made stretching station.

2.3. Results and Discussion

2.3.1 Mechanical characterizations

Figure 2.1 shows the molecular structure of PC, and PI based polymers. To confirm the effect of the amorphous microstructure on the polymer's mechanical properties, atomic force microscopy (AFM), and grazing incidence X-ray diffraction (GIXD) were used (Figure 2.2). Through the nanoindentation analysis the elastic modulus of PC-RA, PC-RR, PI-RA, and PI-RR films were measured (Figure 2.3).[65, 66] The elastic modulus values were calculated through the Oliver and Pharr method.[67] The elastic modulus of PC-RA, PC-RR, PI-RA, and PI-RR were 0.309, 0.568, 1.02, and 2.53 Gpa, respectively. It has been reported that elastic modulus calculated from nanoindentation tends to be almost the same as those calculated from the free-standing tensile test.[42, 67] The regio-regular (RR) polymers have a higher modulus than each regio-random(RA) polymers. The high modulus of RR polymers was attributed to their relatively high crystallinities, and these relatively high crystallinities are because the regular polymer chain configuration makes them more amorphous, which increases the free-volume. In addition, the elastic modulus of the PC based polymers was lower than that of the PI based polymer, which is consistent with the result of GIXD analysis (Figure 2.4, and Table 2.1).

To investigate the polymer film morphology under the mechanical strain, the soft contact lamination method was used to transfer the polymer films from Si wafer to PDMS, and those polymer films were monitored by optical microscopy under the specific strain states using a custom-made stretching device (Figure 2.5).[68-70] For PI-RR films, the diamond-shaped microcracks were observed at 80% strain, and both the crack density and size increased with increasing

strain (**Figure 2.6, 2.7**). When monitoring the PC-RR, and PI-RA films, the diamond shape microcracks were observed at 100% strain states. In contrast, there was no crack in the PC-RA films even at 100% strain. When the films were stretched to 150%, the micro-cracks were observed. To further investigate the chain alignment of polymer films under mechanical strain, the dichroic ratios of each polymer were calculated by using polarized UV/visible spectroscopy (**Figure 2.8**). The dichroic ratio of PC-RA film increased up to 2.1 when the strain increased up to 100% due to its high degree of polymer chain alignment and low elastic modulus. In the case of PC-RR, PI-RA, and PI-RR, the dichroic ratios increased until their crack onset strain (100, 100, and 80% for PC-RR, PI-RA, and PI-RR, respectively), and they were no longer increased after the crack onset strain, which resulted from polymer chain relaxation due to the crack formation under crack onset strain. These results were consistent with optical microscopy analysis results of the polymer films.

2.3.2. Electrical Characteristics of OFETs

To investigate the electrical characteristics of PI, and PC based polymers, bottom-gate top-contact (BGTC) OFETs were fabricated (**Figure 2.9**). The polymer solutions in chloroform (2 mg mL^{-1}) were spin-coated onto SiO2/Si substrates which were modified by n-octadecyltrimethoxysilane (OTS) self-assembled layer (SAM) and then annealed at 100℃ for 10 min. The electrical characteristics of the comparison of the transfer characteristics, electron mobility, and output characteristics in N_2 according to the molecular composition and stereo-regularity respectively (**Figure 2.10**, and **Table 2.2**). All of the polymers exhibited electron-dominant charge transport characteristics. The average electron mobility ($\mu_{e,avg}$) of PI-R, PI-A, PC-R, and PC-A was 1.23×10^{-2}, 1.01×10^{-2}, 5.81×10^{-3}, and 4.75×10^{-3} cm^2 V^{-1}, respectively, and on/off ratios were over the 10^5 for all the copolymers (**Figure 2.11**). Also, to verify the electrical

characteristics and avoid the overestimation issues of charge carrier mobility, the reliability factor (r) was calculated in the saturation regime. The r [%] factor means the ratio of measured FET mobility to ideal FET mobility and the equation as follows (eq 1).[71–73]

$$r = \frac{\mu_{measured}}{\mu_{ideal}} = \frac{\left(\frac{I_{DS,max}{}^{0.5} - I_{DS,0}{}^{0.5}}{V_{G,max} - V_{G,0}}\right)^2}{\left(\frac{WC_{ox}\mu_{ideal}}{2L}\right)} \quad (1)$$

Where $I_{DS,max}$ is measured source–drain current at the maximum gate voltage ($V_{G,max}$), and $I_{DS,0}$ means the source–drain current at the onset gate voltage ($V_{G,0}$). The ideal electron mobility of all the polymers were 2.6×10^{-3} cm^2 V^{-1}, 1.5×10^{-3} cm^2 V^{-1}, 6.45×10^{-3} cm^2 V^{-1}, and 2.93×10^{-3} cm^2 V^{-1} for PI–RR, PI–RA, PC–RR, and PC–RA, respectively. As previously reported, the regio–regular polymers were shown better charge transport properties than regio–random polymers due to their relatively high crystallinity to favor intra–/inter–molecular charge transfer.[74]

2.3.3. Electrical & Optoelectrical Characteristics of PI, and PC polymers based OFETs under Mechanical Strain

To further confirm the electrical properties of PI, and PC based OFETs under mechanical strain, electrical characteristics were estimated with OFETs of which device geometry is BGTC. For the stretched films fabricating, the polymer films which were onto the OTS treated SiO_2/Si wafer were laminated to PDMS (20:1 ratio of base to cross–linker), and the PDMS were stretched with polymer films. After that, these films were laminated on the SiO_2/Si in the N_2 filled glove box by using the soft contact lamination method (**Figure 2.12**). The transfer curves of all the polymers under various mechanical strains (ε, 0–100%) which consist of two directions, perpendicular and parallel directions to the channel were shown that all polymers can maintain their transistor characteristics even at 100% strain (**Figure 2.13**). According to the stretching direction which is parallel or perpendicular to the transistor channel, the mobility

retention tends to be changed. In general, the OFETs stretched parallel to the channel showed higher mobility retention than stretched perpendicular ones due to polymer chain alignment. The polymer chains tend to be aligned along the stretched direction. Thus, high mobility retention in a parallel direction resulted from favored intramolecular charge transfer in parallel direction to channel (**Figure 2.14**). During the electrical characterization under the strain, all the polymers in this study can dissipate the strain energy by deforming the amorphous region, and the rigid backbone of polymers makes the charge transport to be maintained along with the conjugated structures. Therefore, the charge transport pathway can be maintained by the rigid, coplanar, and conjugated backbone of the polymers. Especially, the PC-RA based OFETs show higher electron mobility retention up to 90% at 100% strain in a parallel direction to channel due to its relatively amorphous microstructure and low elastic-modulus. In contrast, PI-RR showed a large mobility decrease which is 11% of initial mobility under the 100% strain and this decrease of mobility resulted from crack propagation. PC-RR, and PI-RA films showed 33%, and 35% mobility retention.

2.4. Conclusion

In conclusion, mechanical characteristics were analyzed according to the regio-regularity of PC, and PI films. Due to the increase of the amorphous region by the chain configuration, the elastic modulus of regio-random polymers was lower than that of regio-regular polymers as 0.309, and 0.568 Gpa for PC based polymers. PI based polymer also show same tendency as 1.02, and 2.53 Gpa, respectively. Optical microscopy monitoring was performed for crack onset strain analysis, and it was confirmed that diamond-shaped micro voids occurred in 150% of PC-RA polymers. In PC-RR, PI-RA, and PI-RR, cracks started to occur at 100, 80, and 100%, respectively. Also, the size and density of the formed micro void cracks increased as the strain increased. Additionally, the dichroic ratio was determined through polarized UV/visible

spectroscopy analysis. PC-RA, whose crack onset was confirmed to be 150%, continued to increase the dichroic ratio up to 2.1 even at 100% strain. The dichroic ratio of PC-RR steadily increased up to 80% strain, and then the slope decreased sharply as it reached 100% strain, which is because of the micro voids found in OM monitoring. PI-RA and PI-RR polymers also showed decreased slope when they reached the crack onset strain as confirmed by OM monitoring, and both PC and PI polymers showed high dichroic ratios at regio-random (RA) polymers. This is because molecular alignment can occur more easily due to the relatively high amorphous. As a result of measuring the electrical properties, the electron mobility of PI-RR, PI-RA, PC-RR, and PC-RA was 1.23×10^{-2}, 1.01×10^{-2}, 5.81×10^{-3}, and $4.75 \times 10^{-3} cm^2 V^{-1}$. In general, regio-regular polymers showed higher mobility than regio-random polymers because charge transfer could be better due to their relatively high crystallinity. After that, the electrical properties retention under the strain. PC-RA stretched in parallel to the channel direction showed an electron mobility retention up to 90% under 100% strain, and PC-RR showed mobility retention up to 33%. PI-RA and PI-RR showed electron mobility retention of 35% and 11% under 100% strain, respectively, which is consistent with the previously measured dichroic ratio, elastic modulus, and crack onset strain results. Through this study, the effect of stereoregularity of novel n-type stretchable polymer semiconductors on changes in mechanical properties and electrical properties of polymer semiconductor materials was characterized.

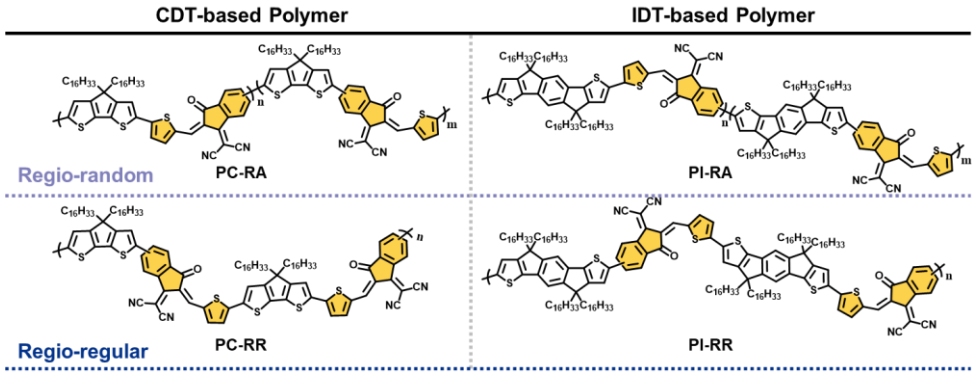

Figure 2.1. Molecular structures of the PCDT-TIC regio-random (PC-RA), PCDT-TIC regio-regular (PC-RR), PIDT-TIC regio-random (PI-RA), and PIDT-TIC regio-regular (PI-RR).

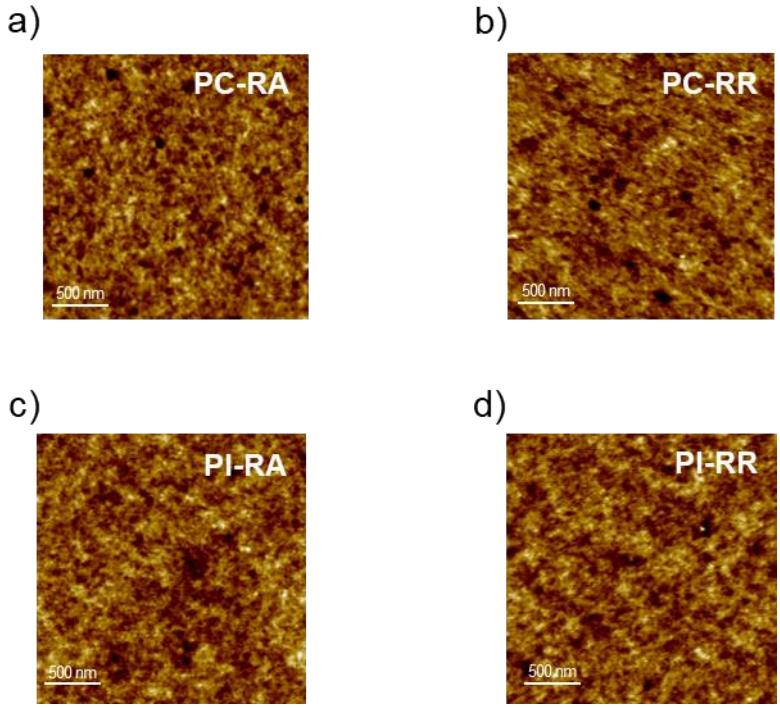

Figure 2.2. AFM height images PC-RA, PC-RR, PI-RA, and PI-RR.

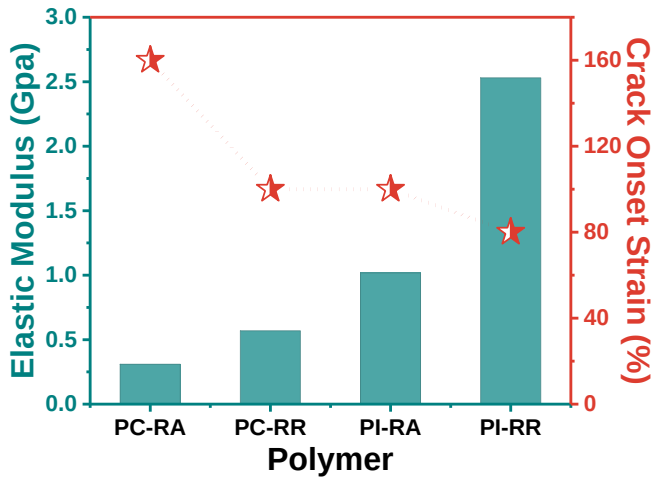

Figure 2.3. Influence of the regio-regularity of polymer on elastic modulus and crack onset strain.

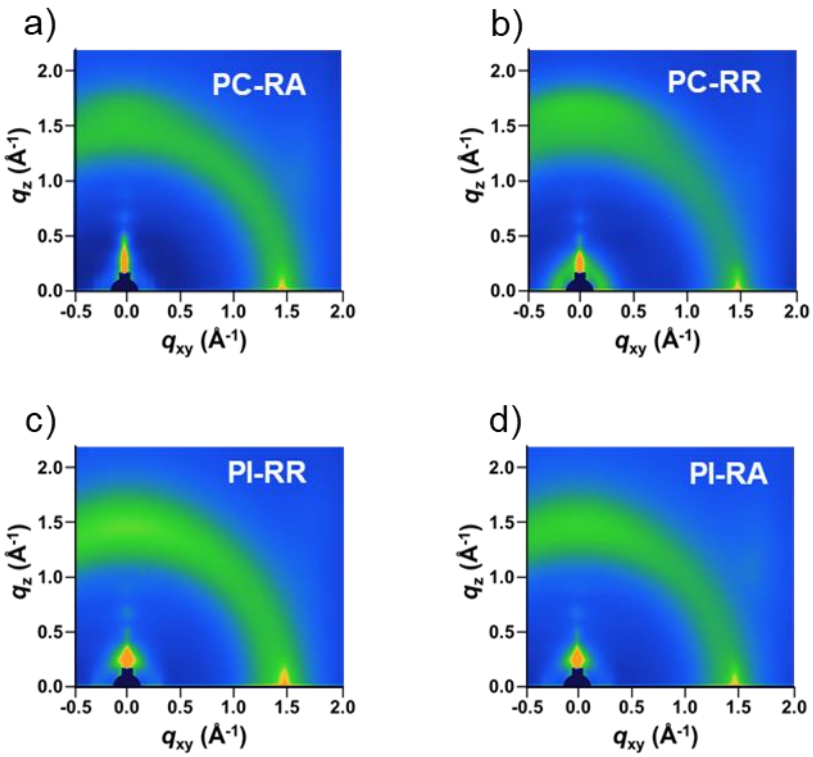

Figure 2.4. GIXD patterns of PC-RA, PC-RR, PI-RR, and PI-RA polymer films.

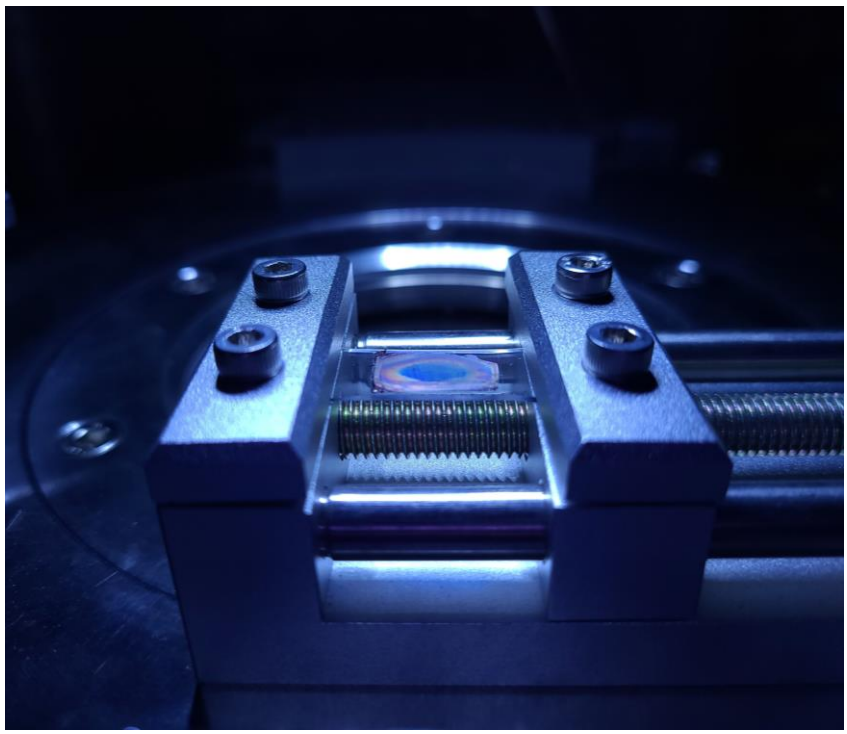

Figure 2.5. Optical image of real stretching test of intrinsically stretchable semiconductor polymer film.

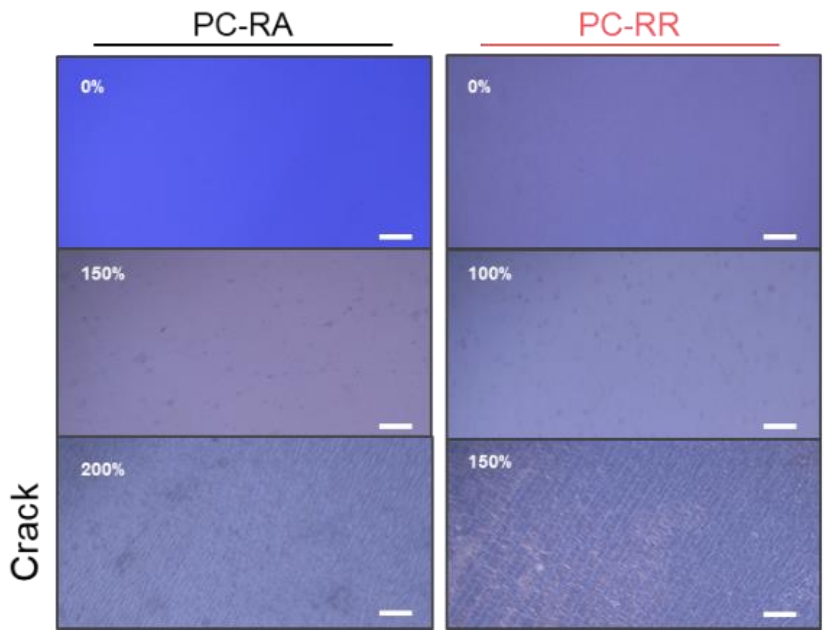

Figure 2.6. Optical images under mechanical strain for finding the crack onset strain of PC-RA, and PC-RR polymer films.

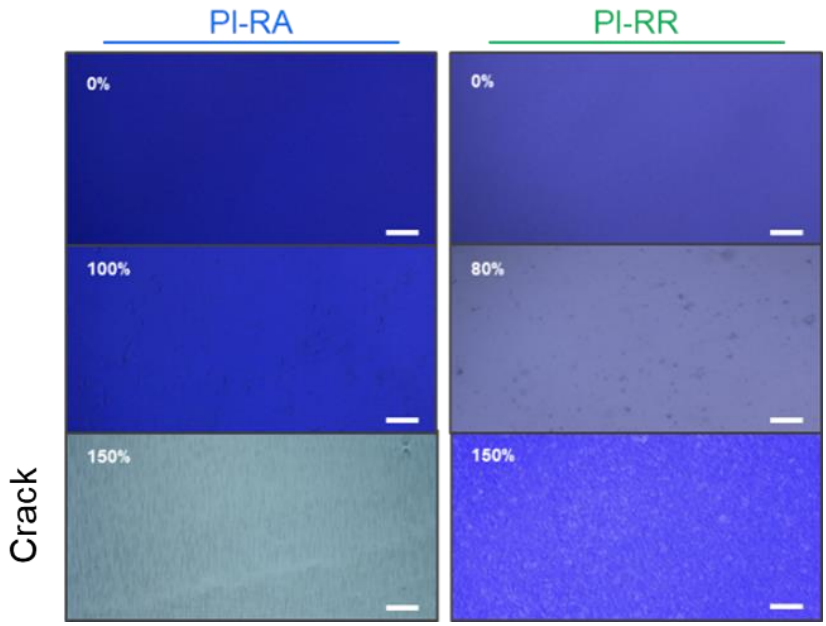

Figure 2.7. Optical images under mechanical strain for finding the crack onset strain of PI-RA, and PI-RR polymer films.

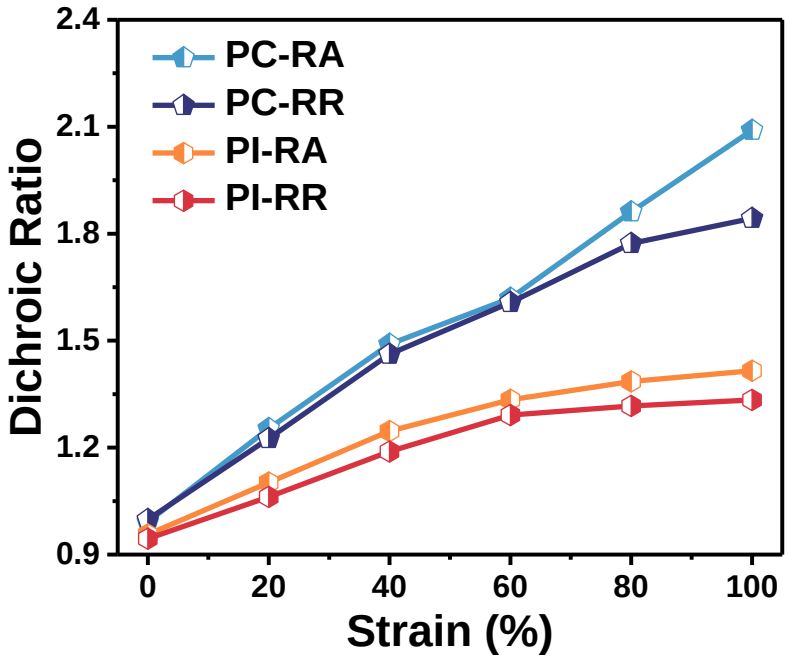

Figure 2.8. Dichroic ratios of PC−RA, PC−RR, PI−RA, and PI−RR.

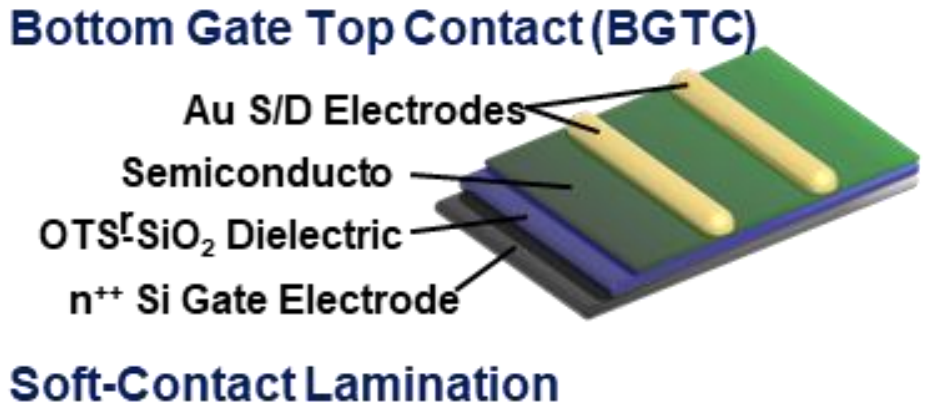

Figure 2.9. Device configuration of OFETs (BGTC).

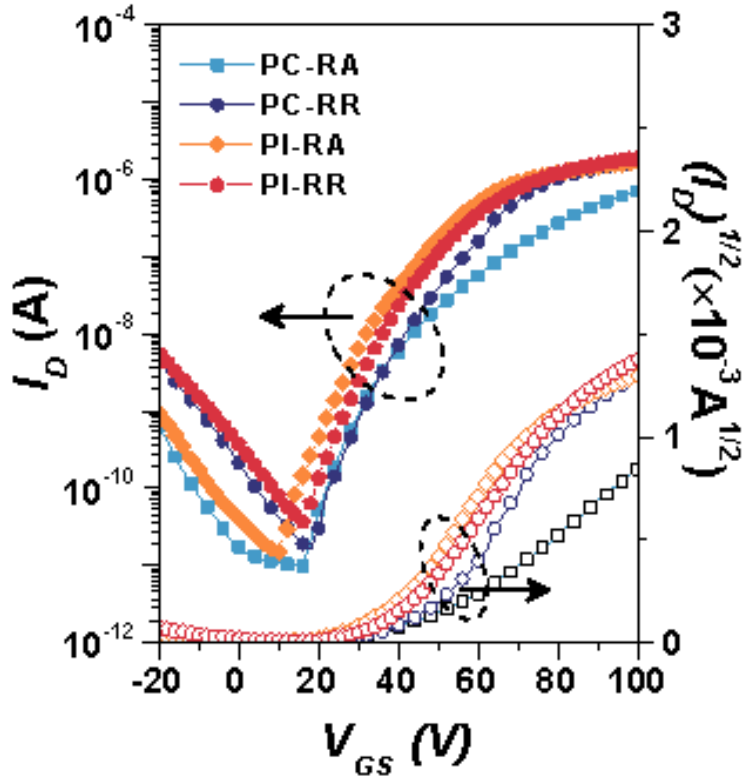

Figure 2.10. N-type transfer characteristics of PC-RA, PC-RR, PI-RA, and PI-RR.

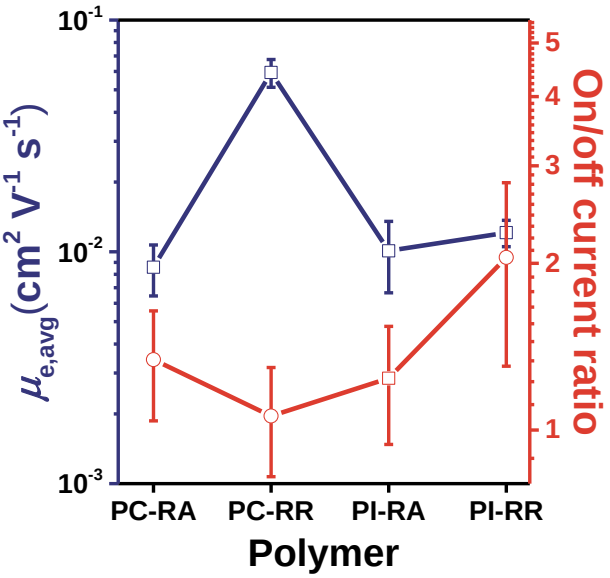

Figure 2.11. Comparison of the electron mobility and on/off ratio of PC-RA, PC-RR, PI-RA, and PI-RR based OFETs.

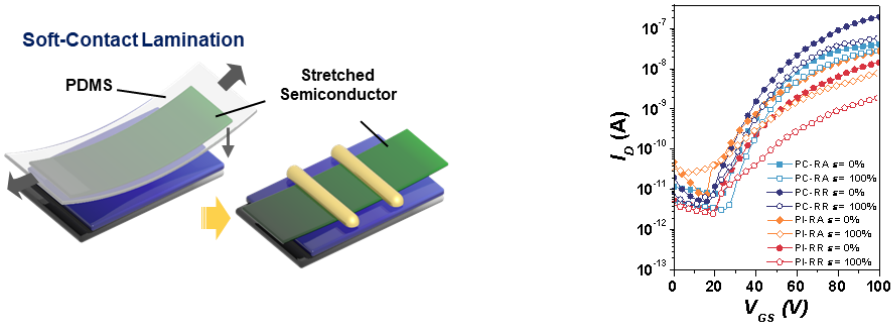

Figure 2.12. Schematic of soft contact lamination process and stretched polymer semiconductor film based OFETs (left), transfer characteristics under mechanical strain (0, and 100% for each polymers).

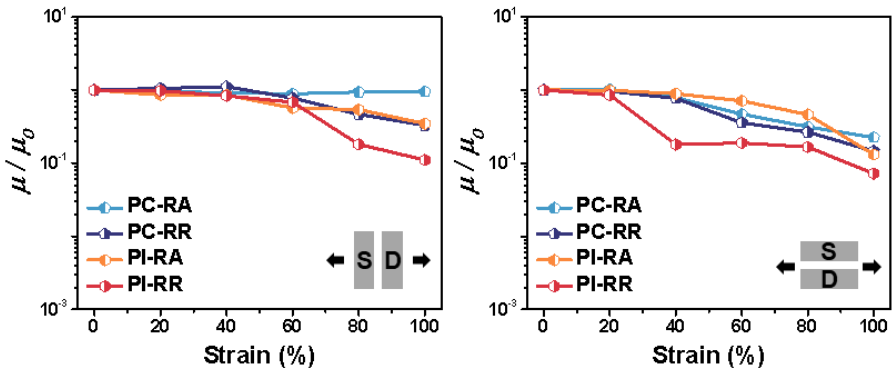

Figure 2.13. Comparison of mobility retention under strain: stretched parallel to channel direction (left), and stretched perpendicular to channel direction (right).

Chapter 3. Optoelectrical Characteristics of Stretchable Organic Phototransistors

3.1. Introduction

With the advent of the 4th industrial revolution and artificial intelligence industry, photo detectors which can be applied as wearable devices form are attractive fields. Especially, in the field of optoelectronic devices, studies have been widely conducted because of their potential for wearable devices and health care devices. [75, 76] The organic semiconducting materials can be applied in wearable or health care devices with lightweight, flexible, stretchable, and easily controllable their optoelectronic properties by molecular design.[77 78, 79] With this nature, various strategies have been revealed over the past year. By using heterojunction structures of organic semiconductor, the photogeneration efficiency has been improved with fulfilling up to 10^{13} Jones.[80] Furthermore, the organic semiconductors has easy absorption wavelength tuning nature, thus allowing wide or high sensitivity to specific wavelengths that from UV−vis to near−infrared (NIR) range.

The photodetector operates by absorbing the energy from the light source and transforming it as an electrical current. The light−induced current increased when the charges are pulled out without recombination.[52 81]

3.2. Experimental Section

3.2.1. Optoelectronic characterization.

The photo−induced I−V characteristics and real−time photo−switching were conducted under vacuum (<5.0 × 10−6 Torr). The optoelectronic properties were measured with a monochromatic light source under vacuum (<5.0 × 10−6 Torr) and Keithley 4200 semiconductor parameter analyzer to characterize the electrical properties of a device.

3.2.2. Photo-switching under the mechanical strain

To fabricate the stretched polymer film based OFETs, the polymer solution (2mg/ml, in chloroform) was stirred overnight at 50℃. After that, the polymer films were formed by spin-coating process onto OTS treated SiO2/Si wafer. These polymer films were transferred onto the PDMS (20:1, base to cross-linker mass ratio), and the films were stretched onto PDMS. Then, these stretched films were directly laminated onto the SiO2/Si wafer by the soft contact lamination method. Under the incident light pulsed at the 20s, the monochromatic light was irradiated to stretched polymer films based on OPTs.

3.3. Results and Discussion

To investigate optoelectronic properties of PI, and PC copolymers, cyclic voltammetric was measured (**Figure 3.1**). **Figure 3.2** shows the HOMO, and LUMO energy levels of PC, and PI based polymers. Also, UV/vis absorption spectra were analyzed to confirm their absorption peak and coefficient (**Figure 3.3**, **Table 3.1**). The organic phototransistors (OPTs) of which the structure is bottom-gate top-contact were fabricated. The lights which consist of various wavelengths and light intensities (λ is from NIR to UV region; intensities are from 10 to 100 μW cm^{-2}) were emitted through a monochromatic light source under a vacuum (below 5.0×10^{-6} Torr). The maximum absorption wavelengths of PI-R, PI-A, PC-R, PC-A (738, 721, 835, 755 nm, respectively) which are shown in **Table 3.1** were selected. When comparing the transfer characteristics of the OPTs upon light irradiation with dark condition, increased drain current which resulted from irradiate the light was found in the PC polymers based OPTs (**Figure 3.4**). In addition, additional photoinduced current increases were observed when the light intensity was increased. To estimate the optoelectronic properties of the PI, and PC based OPTs further, the photocurrent / dark-current

(P), and photoresponsivity were calculated (**Figure 3.5**). Note that the optoelectronic properties of PC polymers were higher than PI polymers OPTs. The enhanced OPTs performance of PC polymers compared to that of PI polymers based OPTs may be related to their high crystallinity, and longer exciton diffusion length, as evident by the larger movement of Von towards the negative direction. The R and P of the PC-RR based OPTs were measured under monochromatic light irradiation ($\lambda \approx 838$ nm, intensity = 60 μW cm^{-2}), and the R and P values were 36 A W-1, and 116 respectively. Also, PC-RR OPTs showed maximum R and P values of 203, and 94, respectively, in the 60 μW cm^{-2} of light irradiation. The EQE and D* values were also estimated to investigate the photo-response behaviors of OPTs. The PC-R based OPTs had EQE, and D^* values of 5282%, and 1.4×10^{12} Jones under the maximum absorption wavelength (838 nm, intensity = 60 μW cm^{-2}), respectively.

Real-time photo-switching properties of all the polymers were measured under pulsed incident light (60 μW cm^{-2}) when the V_{GS} value of 100 V. These V_{GS} correspond to values that the maximum R values were obtained. The calculated rise time (τ_r) and decay time (τ_d) defined as the taking time to reach 90% of the maximum photocurrent and the taking time drop to 10% of the maximum photocurrent, respectively. The PC-R polymer based OPTs were 0.15 s and 0.66 s for the rise, and decay time, respectively (**Figure 3.6**). The shorter response time is an important parameter when the OPTs are integrated with circuits and act as fast response photodetectors. Also, **Figure 3.7** shows that the photocurrents can be amplified by the positive bias. The normalized I_{DS} was nearly 0 at V_{GS} = 0 V but this current was increased dramatically to nearly 100, and 400 when the V_{GS} was 60 V, and 100V, respectively. These results are one of the advantages of the transistor's amplification properties. Using these properties, the OPTs could modulate the photo-responsivity.

The real-time photo-switching behavior of PC-R according to the change of wavelengths was performed under incident light pulsed at 20 s (V_{DS} = 100 V, V_{GS} = 60 V). As a result, due to the low bandgap

of PC-R, the photo-induced currents were shown differently in the same intensities (30 μW cm^{-2}) of various wavelengths which consist from NIR region to UV region (**Figure 3.8**). Also, PC-RR based OPTs showed to keep their photoresponsivity under a mechanical strain up to 100% (**Figure 3.9**)

3.4. Conclusion

In conclusion, the optoelectrical properties were measured. The monochromatic light wavelengths were selected as maximum absorption peaks (755, and 838 nm for PC-RR, and PC-RA, respectively). The R, P, EQE, and D* values of PC-RR and PC-RA at the same light intensity were 36, 116, 5282, 1.4 x 10^{12}, and 1.1, 378, 180, and 4 x 10^{9}, respectively. In particular, in the case of PC-RR, even at a 10 μW cm^{-2}, it showed high optical characteristics (203, 94, 24186, 8.2 x 10^{12} for R, P, EQE, and D*, respectively), and the τ_r and τ_d values also showed a fast response speed of less than 0.15 and 0.66 sec, respectively. In addition, it showed that the photo-response could be improved through amplification, which is an advantage of OPTs, and photoresponsivity showed through real-time photo-switching from the NIR region to the UV region. Finally, by measuring the electrical characterization of stretched film-based OPTs, photoresponsivity could maintain even at the stretched state through real-time photo-switching.

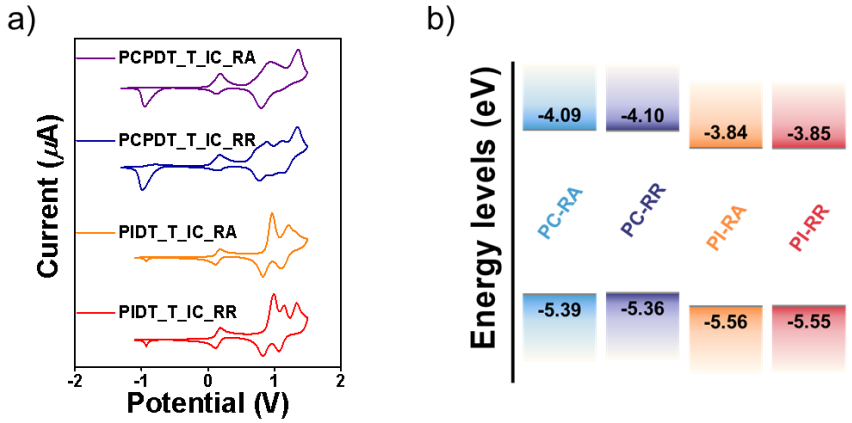

Figure 3.1. a) Cyclic voltametric results of PC-RA, PC-RR, PI-RA, and PI-RR, b) HOMO and LUMO energy levels of PC-RA, PC-RR, PI-RA, and PI-RR.

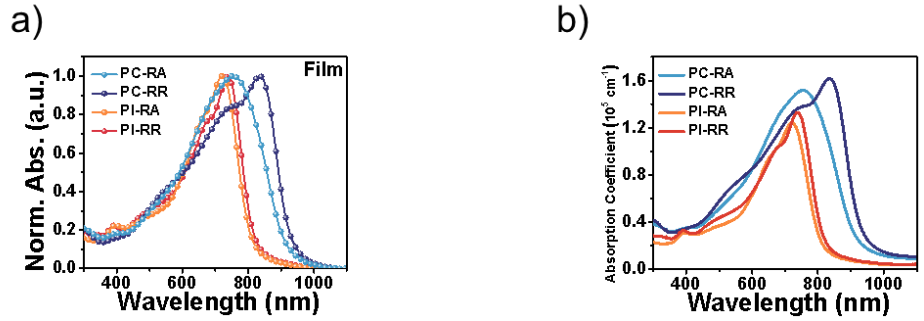

Figure 3.2. a) UV/Vis spectra of PC-RA, PC-RR, PI-RA, and PI-RR films, b) UV/Vis absorption coefficient spectra of PC-RA, PC-RR, PI-RA, and PI-RR.

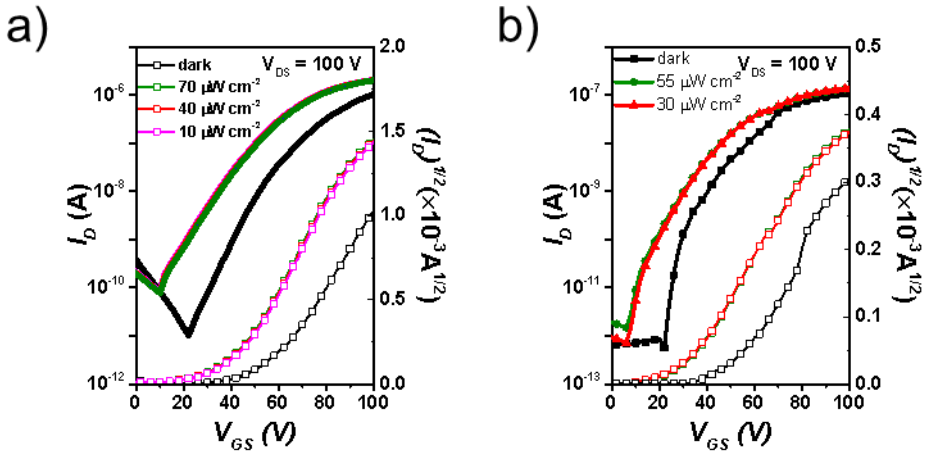

Figure 3.3. Photo-induced transfer characteristics of a) PC-RR, and b) PC-RA under the dark and monochromatic light irradiation.

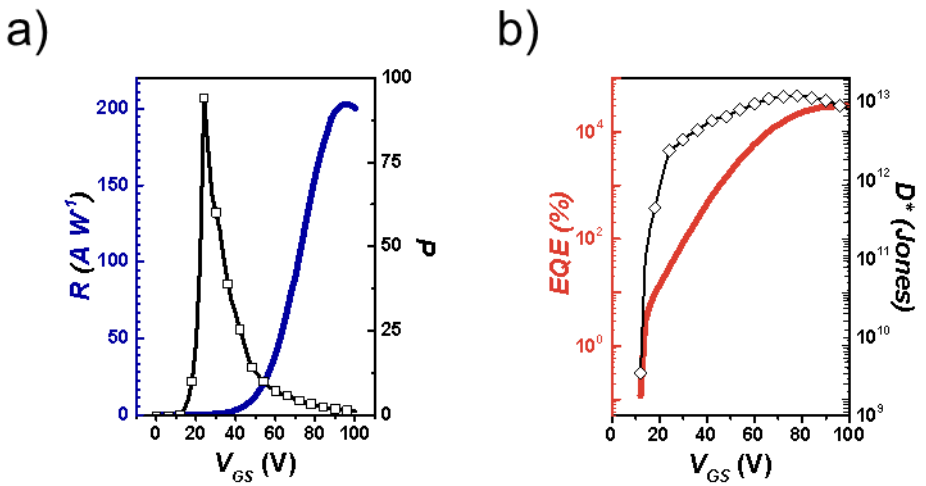

Figure 3.4. Optoelectronic properties of PC-RR based OPTs under 838 nm (10 μW cm^{-2}): a) photo-responsivity (R), and photocurrent/dark-current (P), b) external quantum efficiency (EQE), and detectivity (D^*).

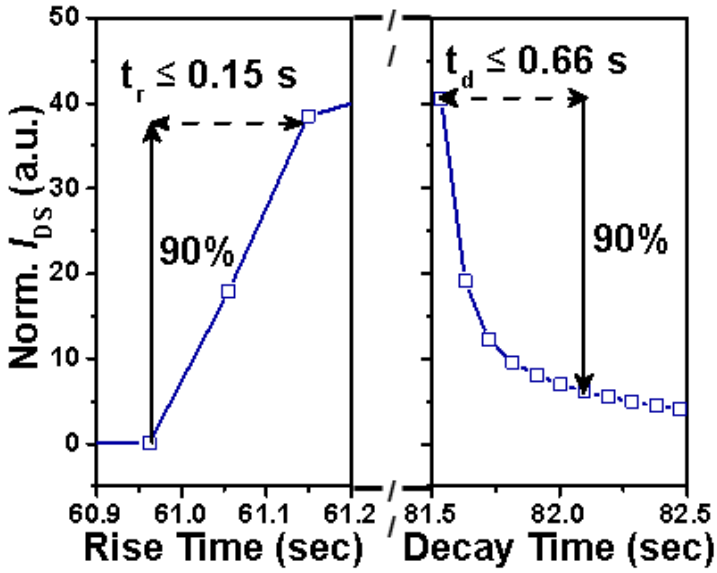

Figure 3.5. Photo-response times PC-RR based OPTs.

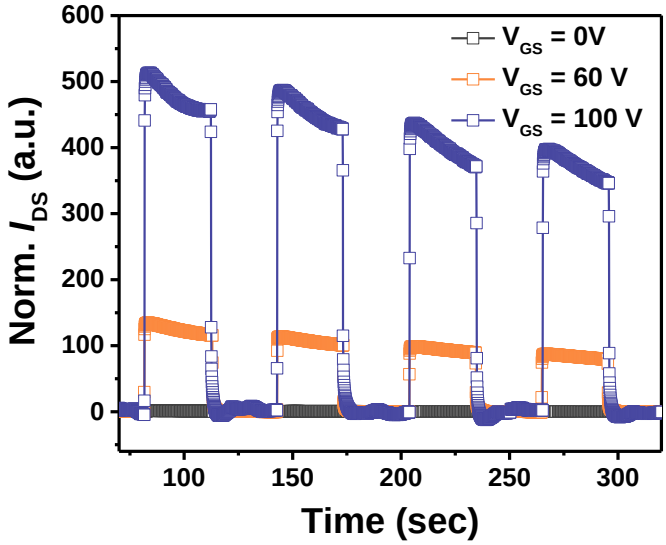

Figure 3.6. PC-RR based OPTs amplificated real-time photo-switching behavior.

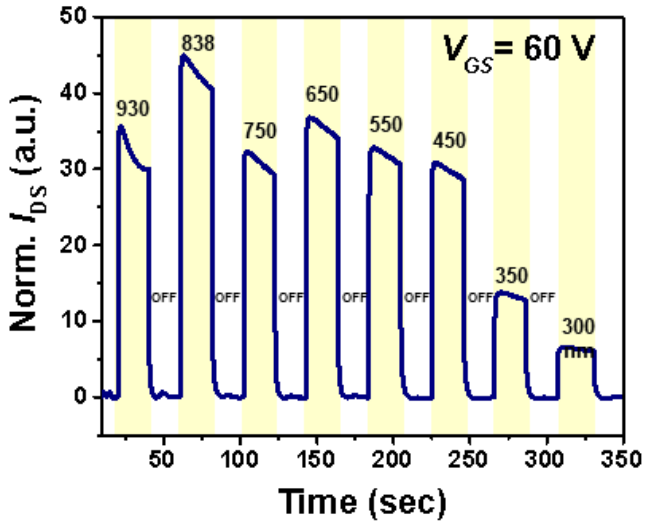

Figure 3.7. Real-time photo-response of PC-RR based OPTs under light irradiation at 20s intervals under various wavelengths from NIR to UV range.

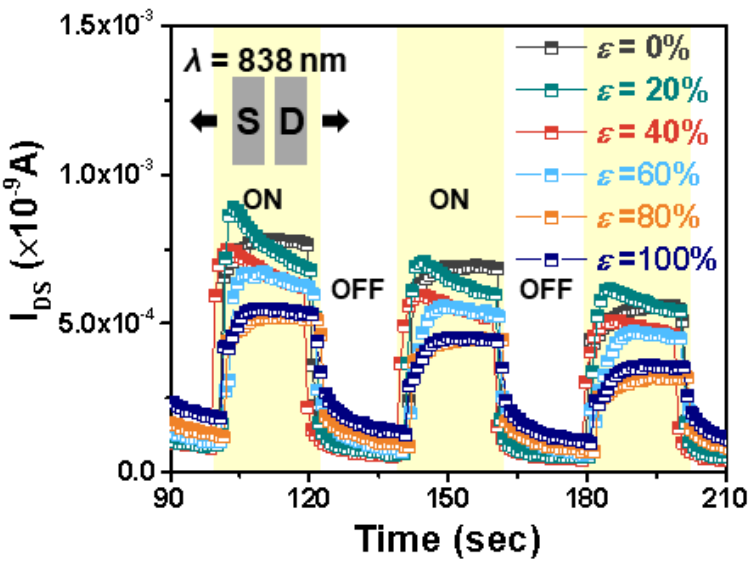

Figure 3.8. Real-time photo-response of PC-RR based OPTs under mechanical strain (0-100%).

Table 2.1. Relevant parameters of PC-RA, PC-RR, PI-RA, and PI-RR polymer films at in-plane directions of GIXD data.

	In-Plane π-π Stacking Cell Axis (010)			
	q (Å^{-1})	d-spacing (Å)	FWHM (Å^{-1})	Coherence length (Å)
PC-RA	1.514	4.149	0.089	64.128
PC-RR	1.514	4.150	0.076	75.268
PI-RA	1.511	4.158	0.081	70.321
PI-RR	1.512	4.157	0.076	75.435

Table 2.2. Summarized electrical characteristics of OFETs based on PIDT-TIC & PCDT-TIC.

Polymers	Type	Average Values				$\mu_{e,avg}$ [cm^2 V^{-1} s^{-1}]
		I_{on} [A]	I_{off} [A]	I_{on}/I_{off}	V_T [V]	
PIDT	RR	1.69 x 10^{-6}	8.24 x 10^{-12}	2.05 x 10^5	29.6	1.21 x 10^{-2}
	RA	1.85 x 10^{-6}	1.49 x 10^{-11}	1.24 x 10^5	34.7	1.01 x 10^{-2}
PCDT	RR	2.14 x 10^{-6}	1.59 x 10^{-11}	1.34 x 10^5	12.7	5.94 x 10^{-2}
	RA	1.02 x 10^{-6}	9.59 x 10^{-12}	1.06 x 10^5	14.1	8.58 x 10^{-3}

Table 3.1. Optical and electrophysical properties of PC−RA, PC−RR, PI−RA, and PI−RR.

	λ_{sol}^{max} [nm][a]	λ_{film}^{max} [nm][a]	λ_{onset} [nm][b]	E_g^{opt} [eV][b]	E_{HOMO}^{CV} [eV][c]	E_{LUMO}^{CV} [eV][c]	Mn [kDa]	PDI
PC-RA	763	755	918	1.35	-5.39	-4.09	40.8	2.43
PC-RR	843	835	933	1.33	-5.36	-4.10	44.2	2.30
PI-RA	733	721	811	1.53	-5.56	-3.84	69.8	1.65
PI-RR	745	738	823	1.51	-5.55	-3.85	72.1	1.63

Table 3.2. Optoelectronic Properties of PI and PC based OPTs.

Polymer	λ_{sol}^{max} [nm][a]	Light intensity [μW cm-2]	R [A W^{-1}]	P	EQE, η [%]	D^* [Jones]
PI –RR	738	60	10	1650	1711	1.5×10^{12}
PI-RA	721	60	1.3	1740	235	4.7×10^{11}
PC-RR	838	10	203	94	24186	8.12×10^{12}
PC-RR	838	60	36	116	5282	1.4×10^{12}
PC-RA	755	55	1.1	378	180	4×10^{9}

References

1. Braga D, Horowitz G. High-Performance Organic Field-Effect Transistors. *Advanced Materials* **21**, 1473-1486 (2009).

2. Kang B, *et al.* Enhancing 2D growth of organic semiconductor thin films with macroporous structures via a small-molecule heterointerface. *Nature Communications* **5**, 4752 (2014).

3. Knopfmacher O, *et al.* Highly stable organic polymer field-effect transistor sensor for selective detection in the marine environment. *Nature Communications* **5**, 2954 (2014).

4. Dimitrakopoulos CD, Mascaro DJ. Organic thin-film transistors: A review of recent advances. *IBM Journal of Research and Development* **45**, 11-27 (2001).

5. Kim J, Han AR, Seo JH, Oh JH, Yang C. β-Alkyl substituted Dithieno[2,3-d;2′,3′-d′]benzo[1,2-b;4,5-b′]dithiophene Semiconducting Materials and Their Application to Solution-Processed Organic Transistors. *Chemistry of Materials* **24**, 3464-3472 (2012).

6. Oh JH, *et al.* Solution-processed, high-performance n-channel organic microwire transistors. *Proceedings of the National Academy of Sciences* **106**, 6065 (2009).

7. Yu H, Bao Z, Oh JH. High-Performance Phototransistors Based on Single-Crystalline n-Channel Organic Nanowires and Photogenerated Charge-Carrier Behaviors. *Adv Funct Mater* **23**, 629-639 (2013).

8. Yu H, Joo P, Lee D, Kim B-S, Oh JH. Photoinduced Charge-Carrier Dynamics of Phototransistors Based on Perylene Diimide/Reduced Graphene Oxide Core/Shell p–n Junction Nanowires. *Advanced Optical Materials* **3**, 241-247 (2015).

9. Mushrush M, Facchetti A, Lefenfeld M, Katz HE, Marks TJ. Easily processable phenylene-thiophene-based organic field-effect transistors and solution-fabricated nonvolatile transistor memory elements. *Journal of the American Chemical Society* **125**, 9414-9423 (2003).

10. Baeg K-J, *et al.* High-Performance Top-Gated Organic Field-Effect Transistor Memory using Electrets for Monolithic Printed Flexible NAND Flash Memory. *Adv Funct Mater* **22**, 2915-2926 (2012).

11. Baeg KJ, Noh YY, Ghim J, Kang SJ, Lee H, Kim DY. Organic Non-Volatile Memory Based on Pentacene Field-Effect Transistors Using a Polymeric Gate Electret. *Advanced Materials* **18**, 3179-3183 (2006).

12. Torsi L, Magliulo M, Manoli K, Palazzo G. Organic field-effect transistor sensors: a tutorial review. *Chemical Society Reviews* **42**, 8612-8628 (2013).

13. Cho YJ, Kim OY, Lee JY. Synthesis of an aromatic amine derivative with novel double spirobifluorene core and its application as a hole transport material. *Organic Electronics* **13**, 351-355 (2012).

14. Lipomi DJ, *et al.* Skin-like pressure and strain sensors based on transparent elastic films of carbon nanotubes. *Nature Nanotechnology* **6**, 788-792 (2011).

15. Ozin GA, *et al.* Nanofabrication by self-assembly. *Materials Today* **12**, 12-23 (2009).

16. Zheng Y, *et al.* An Intrinsically Stretchable High-Performance Polymer Semiconductor with Low Crystallinity. *Adv Funct Mater* **29**, 1905340 (2019).

17. Oh JY, *et al.* Intrinsically stretchable and healable semiconducting polymer for organic transistors. *Nature* **539**, 411-415 (2016).

18. Yu KJ, Yan Z, Han M, Rogers JA. Inorganic semiconducting materials for flexible and stretchable electronics. *npj Flexible Electronics* **1**, 4 (2017).

19. Inal S, Rivnay J, Suiu AO, Malliaras GG, McCulloch I. Conjugated Polymers in Bioelectronics. *Accounts of chemical research* **51**, 1368-1376 (2018).

20. Root SE, Savagatrup S, Printz AD, Rodriquez D, Lipomi DJ. Mechanical Properties of Organic Semiconductors for Stretchable, Highly Flexible, and Mechanically Robust Electronics. *Chemical Reviews* **117**, 6467–6499 (2017).

21. Wang G-JN, Gasperini A, Bao Z. Stretchable Polymer Semiconductors for Plastic Electronics. *Advanced Electronic Materials* **4**, 1700429 (2018).

22. Qian Y, *et al.* Stretchable Organic Semiconductor Devices. *Advanced Materials* **28**, 9243–9265 (2016).

23. Liang J, Li L, Niu X, Yu Z, Pei Q. Elastomeric polymer light-emitting devices and displays. *Nature Photonics* **7**, 817–824 (2013).

24. Kaltenbrunner M, *et al.* Ultrathin and lightweight organic solar cells with high flexibility. *Nature Communications* **3**, 770 (2012).

25. Kaltenbrunner M, *et al.* An ultra-lightweight design for imperceptible plastic electronics. *Nature* **499**, 458–463 (2013).

26. Someya T, Kaltenbrunner M, Yokota T. Ultraflexible organic electronics. *MRS Bulletin* **40**, 1130–1137 (2015).

27. Chortos A, *et al.* Highly Stretchable Transistors Using a Microcracked Organic Semiconductor. *Advanced Materials* **26**, 4253–4259 (2014).

28. Yu Y, *et al.* Three-dimensional compressible and stretchable conductive composites. *Advanced materials (Deerfield Beach, Fla)* **26**, 810–815 (2014).

29. Chen Z, Ren W, Gao L, Liu B, Pei S, Cheng HM. Three-dimensional flexible and conductive interconnected graphene networks grown by chemical vapour deposition. *Nat Mater* **10**, 424–428 (2011).

30. Sekitani T, Noguchi Y, Hata K, Fukushima T, Aida T, Someya T. A rubberlike stretchable active matrix using elastic conductors. *Science (New York, NY)* **321**, 1468–1472 (2008).

31. Sekitani T, *et al.* Stretchable active-matrix organic light-emitting diode display using printable elastic conductors. *Nat Mater* **8**, 494-499 (2009).

32. Yu Z, Niu X, Liu Z, Pei Q. Intrinsically Stretchable Polymer Light-Emitting Devices Using Carbon Nanotube-Polymer Composite Electrodes. *Advanced Materials* **23**, 3989-3994 (2011).

33. Shin M, *et al.* Polythiophene nanofibril bundles surface-embedded in elastomer: a route to a highly stretchable active channel layer. *Advanced materials (Deerfield Beach, Fla)* **27**, 1255-1261 (2015).

34. Lipomi DJ, Lee JA, Vosgueritchian M, Tee BCK, Bolander JA, Bao Z. Electronic Properties of Transparent Conductive Films of PEDOT:PSS on Stretchable Substrates. *Chemistry of Materials* **24**, 373-382 (2012).

35. Guo CF, Sun T, Liu Q, Suo Z, Ren Z. Highly stretchable and transparent nanomesh electrodes made by grain boundary lithography. *Nature Communications* **5**, 3121 (2014).

36. Fukuda K, Takeda Y, Mizukami M, Kumaki D, Tokito S. Fully Solution-Processed Flexible Organic Thin Film Transistor Arrays with High Mobility and Exceptional Uniformity. *Scientific Reports* **4**, 3947 (2014).

37. Kim RH, *et al.* Waterproof AlInGaP optoelectronics on stretchable substrates with applications in biomedicine and robotics. *Nat Mater* **9**, 929-937 (2010).

38. Kim DH, Ghaffari R, Lu N, Rogers JA. Flexible and stretchable electronics for biointegrated devices. *Annual review of biomedical engineering* **14**, 113-128 (2012).

39. O'Connor B, *et al.* Correlations between mechanical and electrical properties of polythiophenes. *ACS Nano* **4**, 7538-7544 (2010).

40. Ashizawa M, Zheng Y, Tran H, Bao Z. Intrinsically stretchable conjugated polymer semiconductors in field effect transistors.

Progress in Polymer Science **100**, 101181 (2020).

41. Xu J, *et al.* Highly stretchable polymer semiconductor films through the nanoconfinement effect. *Science (New York, NY)* **355**, 59 (2017).

42. Lee MY, Dharmapurikar S, Lee SJ, Cho Y, Yang C, Oh JH. Regular H-Bonding-Containing Polymers with Stretchability up to 100% External Strain for Self-Healable Plastic Transistors. *Chemistry of Materials* **32**, 1914-1924 (2020).

43. Oh JY, *et al.* Stretchable self-healable semiconducting polymer film for active-matrix strain-sensing array. *Science Advances* **5**, eaav3097 (2019).

44. Mun J, *et al.* Effect of Nonconjugated Spacers on Mechanical Properties of Semiconducting Polymers for Stretchable Transistors. *Adv Funct Mater* **28**, 1804222 (2018).

45. Lei T, Wang J-Y, Pei J. Design, Synthesis, and Structure-Property Relationships of Isoindigo-Based Conjugated Polymers. *Accounts of chemical research* **47**, 1117-1126 (2014).

46. Wang G-JN, *et al.* Inducing Elasticity through Oligo-Siloxane Crosslinks for Intrinsically Stretchable Semiconducting Polymers. *Adv Funct Mater* **26**, 7254-7262 (2016).

47. Mei J, Bao Z. Side Chain Engineering in Solution-Processable Conjugated Polymers. *Chemistry of Materials* **26**, 604-615 (2014).

48. Zhao X, *et al.* Complementary Semiconducting Polymer Blends: Influence of Side Chains of Matrix Polymers. *Macromolecules* **50**, 6202-6209 (2017).

49. Chortos A, Liu J, Bao Z. Pursuing prosthetic electronic skin. *Nat Mater* **15**, 937-950 (2016).

50. McCoul D, Hu W, Gao M, Mehta V, Pei Q. Recent Advances in Stretchable and Transparent Electronic Materials. *Advanced Electronic Materials* **2**, 1500407 (2016).

51. Lee Y, Shin M, Thiyagarajan K, Jeong U. Approaches to Stretchable Polymer Active Channels for Deformable Transistors. *Macromolecules* **49**, 433–444 (2016).

52. Chow PCY, Bayliss SL, Lakhwani G, Greenham NC, Friend RH. In Situ Optical Measurement of Charge Transport Dynamics in Organic Photovoltaics. *Nano Letters* **15**, 931–935 (2015).

53. Ren H, Chen J–D, Li Y–Q, Tang J–X. Recent Progress in Organic Photodetectors and their Applications. *Advanced Science* **8**, 2002418 (2021).

54. Baeg K–J, Binda M, Natali D, Caironi M, Noh Y–Y. Organic Light Detectors: Photodiodes and Phototransistors. *Advanced Materials* **25**, 4267–4295 (2013).

55. Wakayama Y, Hayakawa R, Seo H–S. Recent progress in photoactive organic field–effect transistors. *Science and Technology of Advanced Materials* **15**, 024202 (2014).

56. Kumar B, Kaushik BK, Negi YS. Organic Thin Film Transistors: Structures, Models, Materials, Fabrication, and Applications: A Review. *Polymer Reviews* **54**, 33–111 (2014).

57. Zhang Y, *et al.* Ultrasensitive photodetectors exploiting electrostatic trapping and percolation transport. *Nature Communications* **7**, 11924 (2016).

58. Han T, *et al.* Ultrahigh photosensitive organic phototransistors by photoelectric dual control. *Journal of Materials Chemistry C* **7**, 4725–4732 (2019).

59. Luo L–B, *et al.* A Highly Sensitive Perovskite/Organic Semiconductor Heterojunction Phototransistor and Its Device Optimization Utilizing the Selective Electron Trapping Effect. *Advanced Optical Materials* **7**, 1900272 (2019).

60. Charron BP, Ocheje MU, Selivanova M, Hendsbee AD, Li Y, Rondeau–Gagné S. Electronic properties of isoindigo–based conjugated polymers bearing urea–containing and linear alkyl side chains. *Journal of Materials Chemistry C* **6**, 12070–12078 (2018).

61. Ocheje MU, Charron BP, Nyayachavadi A, Rondeau-Gagné S. Stretchable electronics: recent progress in the preparation of stretchable and self-healing semiconducting conjugated polymers. *Flexible and Printed Electronics* **2**, 043002 (2017).

62. Oh JY, *et al.* Intrinsically stretchable and healable semiconducting polymer for organic transistors. *Nature* **539**, 411-415 (2016).

63. Xu J, *et al.* Multi-scale ordering in highly stretchable polymer semiconducting films. *Nature Materials* **18**, 594-601 (2019).

64. Wu H-C, *et al.* A Rapid and Facile Soft Contact Lamination Method: Evaluation of Polymer Semiconductors for Stretchable Transistors. *Chemistry of Materials* **26**, 4544-4551 (2014).

65. Hu Z. Chapter 6 - Characterization of Materials, Nanomaterials, and Thin Films by Nanoindentation. In: *Microscopy Methods in Nanomaterials Characterization* (eds Thomas S, Thomas R, Zachariah AK, Mishra RK). Elsevier (2017).

66. Ditte K, *et al.* Ultrasoft and High-Mobility Block Copolymers for Skin-Compatible Electronics. *Advanced Materials* **33**, 2005416 (2021).

67. Oliver WC, Pharr GM. An improved technique for determining hardness and elastic modulus using load and displacement sensing indentation experiments. *Journal of Materials Research* **7**, 1564-1583 (1992).

68. Hsu LC, *et al.* Highly Stretchable Semiconducting Polymers for Field-Effect Transistors through Branched Soft-Hard-Soft Type Triblock Copolymers. *Macromolecules* **53**, 7496-7510 (2020).

69. Hsu LC, *et al.* Stretchable OFET Memories: Tuning the Morphology and the Charge-Trapping Ability of Conjugated Block Copolymers through Soft Segment Branching. *ACS Applied Materials and Interfaces* **13**, 2932-2943 (2021).

70. Mun J, *et al.* Effect of Nonconjugated Spacers on Mechanical

Properties of Semiconducting Polymers for Stretchable Transistors. *Adv Funct Mater* **28**, (2018).

71. McCulloch I, Salleo A, Chabinyc M. Avoid the kinks when measuring mobility. *Science (New York, NY)* **352**, 1521 (2016).

72. Pei K, Chen M, Zhou Z, Li H, Chan PKL. Overestimation of Carrier Mobility in Organic Thin Film Transistors Due to Unaccounted Fringe Currents. *ACS Applied Electronic Materials* **1**, 379–388 (2019).

73. Bittle EG, Basham JI, Jackson TN, Jurchescu OD, Gundlach DJ. Mobility overestimation due to gated contacts in organic field–effect transistors. *Nature Communications* **7**, 10908 (2016).

74. Himmelberger S, Vandewal K, Fei Z, Heeney M, Salleo A. Role of Molecular Weight Distribution on Charge Transport in Semiconducting Polymers. *Macromolecules* **47**, 7151–7157 (2014).

75. Khan Y, Ostfeld AE, Lochner CM, Pierre A, Arias AC. Monitoring of Vital Signs with Flexible and Wearable Medical Devices. *Advanced materials (Deerfield Beach, Fla)* **28**, 4373–4395 (2016).

76. Khan Y, Ostfeld AE, Lochner CM, Pierre A, Arias AC. Monitoring of Vital Signs with Flexible and Wearable Medical Devices. *Advanced Materials* **28**, 4373–4395 (2016).

77. Jansen–van Vuuren RD, Armin A, Pandey AK, Burn PL, Meredith P. Organic Photodiodes: The Future of Full Color Detection and Image Sensing. *Advanced Materials* **28**, 4766–4802 (2016).

78. Wang H*, et al.* A Retina–Like Dual Band Organic Photosensor Array for Filter–Free Near–Infrared–to–Memory Operations. *Advanced Materials* **29**, 1701772 (2017).

79. Pierre A, Arias AC. Solution–processed image sensors on flexible substrates. *Flexible and Printed Electronics* **1**, 043001 (2016).

80. García de Arquer FP, Armin A, Meredith P, Sargent EH. Solution-processed semiconductors for next-generation photodetectors. *Nature Reviews Materials* **2**, 16100 (2017).

81. Vandewal K. Interfacial Charge Transfer States in Condensed Phase Systems. *Annual Review of Physical Chemistry* **67**, 113-133 (2016).

Abstract in Korean

입체 규칙성은 고분자의 미세구조를 변화시킴으로써 전기적, 기계적, 광학적 특성에 영향을 줄 수 있다. 이 연구에서는, 신규 N-type 고분자 반도체인 PCDT-TIC와 PIDT-TIC를 합성하였으며, 입체규칙성이 물질의 다양한 특성에 미치는 영향을 분석했다. 전기적 특성의 경우, regio-regular (RR) 고분자들의 상대적으로 높은 결정화도로 인해 전하 이동이 유리하기 때문에 regio-random (RA) 고분자들보다 우수한 전기 이동도를 보였다(PC-RR과 PC-RA에서 각각 5.9×10^{-2}, 8.6×10^{-2} $cm^2 V^{-1} s^{-1}$, 그리고 PI-RR과 PI-RA에서 각각 1.2×10^{-2}, 1.0×10^{-2} $cm^2 V^{-1} s^{-1}$). 기계적 특성의 경우 RA 고분자들이 RR 고분자들보다 탄성 모듈러스가 확연히 낮게 나왔으며, PC-RR은 100%에서 다이아몬드 형태의 미세 구멍이 생긴 반면에 PC-RA는 150%에서 발생하는 것을 확인하였다. 더 나아가 100% 늘린 고분자 필름으로 유기 전계 효과 트랜지스터를 제작하여 전기적 특성을 평가결과, PC-RR과 PC-RA는 각각 90%, 33%의 전자 이동도 유지율을 보였다. 또한 광학적 특성에서는 PC-RR이 PC-RA보다 높은 R, EQE, D^*를 보여줬다. 특히, PC-RR 고분자 기반 photo-transistor는 NIR 파장에 대한 높은 광응답성을 보이며 신축 상태에서도 광특성을 유지할 수 있었다.

Acknowledgements

2019년 1월부터 2021년 8월까지, 소중했던 동료들과의 추억에 감사하며 한 말씀 올리겠습니다. 따뜻했던 배려 잊지않겠습니다. 또한 소중한 추억들 잘 간직하고 갑니다. 우리 OPEL 여러분들, 졸업한 후에도 오래오래 연락할 수 있는 사이로 발전해나갈 수 있으면 좋겠습니다. 우울증, 무기력함 등에 빠져서 인생의 큰 시련에 좌절하고 아무것도 해낼 수 없을 것 같은 불안함에서 나를 빠져나올 수 있게 해준 소중한 친구들, 그리고 부모님께 감사합니다. 그리고 다시 한번 포기하지 않으면 언젠가 이룰 수 있다는 사실을 깨닫습니다. 대한민국 최고 학교인 서울대학교 석사를 졸업한 종민아, 앞으로의 목표 잘 정해서 커리어적으로나 인간적으로나 즐길 수 있는 인생 살아가자. 되돌아봤을 때 이 정도면 즐겁게 잘 살았다고 느낄 수 있도록 내 인생 멋있게 꾸며가자. 재우야 네가 만족하는 삶을 살아가면 좋겠다. 울산이라도 네가 행복하다면 난 그거로 족하다. 하지만 그게 아니라면 수원으로 좀 와라. 내가 인생 즐겁게 해줄 수 있다. 건주야 너는 뭐 내가 딱히 이래라 저래라 할 게 없다. 앞으로도 승승장구할 게 뻔하다. 성공해서 나 좀 잘 챙겨줘라. 나의 노년 인생은 네 회사에서 편하게 다녀도 되겠지? 동탄에서 재우랑 너랑 나랑 살면서 자식들끼리도 친하게 지내는게 내 인생 마지막 버킷리스트다. 같이 즐거운 인생 살아보자. 마지막으로 사랑하는 부모님께, 저 그래도 우리나라 최고의 대학 나와서 반도체 시장 세계 1위 기업인 삼성전자에서 기술 개발하는 연구원이 됐습니다. 자랑스러운 아들 두셨네요. 힘들 때마다 자랑스러운 자식이 되고 싶다는 일념으로 이렇게 악으로 깡으로 버텨서 이뤄낼 수 있었습니다. 남부럽지 않은 학교, 남부럽지 않은 회사에 갔으니, 이제는 남부럽지 않게 인생 설계 해볼게요. 잘 지켜봐 주시고 오래오래 건강하게 자식 성장해가는 것 지켜보세요. 그리고 자식이 부모의 마음을 온전히 이해할 수 있는 날 함께 얘기 나누며 지낼 수 있으면 좋겠습니다. 사랑합니다.